Heliyon 10 (2024) e27963

Contents lists available at ScienceDirect

Heliyon

journal homepage: www.cell.com/heliyon

Research article

Time-dependent CT score-based model for identifying severe/critical COVID-19 at a fever clinic after the emergence of Omicron variant

Zhenchen Zhu [a,1], Ge Hu [b,1], Zhoumeng Ying [a,c], Jinhua Wang [a], Wei Han [d], Zhengsong Pan [a,c], Xinlun Tian [e], Wei Song [a], Xin Sui [a], Lan Song [a,*,2], Zhengyu Jin [a,**,2]

[a] *Department of Radiology, Peking Union Medical College Hospital, Chinese Academy of Medical Sciences and Peking Union Medical College, Beijing, China*
[b] *Medical Research Center, Peking Union Medical College Hospital, Chinese Academy of Medical Sciences and Peking Union Medical College, Beijing, China*
[c] *4+4 Medical Doctor Program, Chinese Academy of Medical Sciences and Peking Union Medical College, Beijing, China*
[d] *Department of Epidemiology and Biostatistics, Institute of Basic Medicine Sciences, Chinese Academy of Medical Sciences and Peking Union Medical College, Beijing, China*
[e] *Department of Respiratory and Critical Care Medicine, Peking Union Medical College Hospital, Chinese Academy of Medical Sciences and Peking Union Medical College, Beijing, China*

ARTICLE INFO

Keywords:
COVID-19
Computed tomography
SARS-CoV-2
CT score
Fever clinic

ABSTRACT

Rationale and objectives: The computed tomography (CT) score has been used to evaluate the severity of COVID-19 during the pandemic; however, most studies have overlooked the impact of infection duration on the CT score. This study aimed to determine the optimal cutoff CT score value for identifying severe/critical COVID-19 during different stages of infection and to construct corresponding predictive models using radiological characteristics and clinical factors. *Materials and methods:* This retrospective study collected consecutive baseline chest CT images of confirmed COVID-19 patients from a fever clinic at a tertiary referral hospital from November 28, 2022, to January 8, 2023. Cohorts were divided into three subcohorts according to the time interval from symptom onset to CT examination at the hospital: early phase (0–3 days), intermediate phase (4–7 days), and late phase (8–14 days). The binary endpoints were mild/moderate and severe/critical infection. The CT scores and qualitative CT features were manually evaluated. A logistic regression analysis was performed on the CT score as determined by a visual assessment to predict severe/critical infection. Receiver operating characteristic analysis was performed and

Abbreviations: RSNA, Radiological Society of North America; COVID-19, coronavirus disease; ICU, intensive care unit; MVT, mechanical ventilator; hsCRP, high sensitivity C-reactive protein; NLR, neutrophil-to-lymphocyte ratio; PLR, platelet-to-lymphocyte ratio; ROC, receiver operating characteristic curve; AUC, area under the curve; OR, odds ratio; CI, confidence interval.

* Corresponding author. Department of Radiology, Peking Union Medical College Hospital, Chinese Academy of Medical Sciences and Peking Union Medical College, No. 1 Shuaifuyuan, Dongcheng District, Beijing, 100730, China.

** Corresponding author. Department of Radiology, Peking Union Medical College Hospital, Chinese Academy of Medical Sciences and Peking Union Medical College, No. 1 Shuaifuyuan, Dongcheng District, Beijing, 100730, China.

E-mail addresses: songl@pumch.cn (L. Song), jinzy@pumch.cn (Z. Jin).

[1] Zhenchen Zhu and Ge Hu contributed equally to this work.

[2] Lan Song and Zhengyu Jin contributed equally to this work.

https://doi.org/10.1016/j.heliyon.2024.e27963
Received 19 July 2023; Received in revised form 22 February 2024; Accepted 8 March 2024
Available online 25 March 2024

the area under the curve (AUC) was calculated. The optimal cutoff value was determined by maximizing the Youden index in each subcohort. A radiology score and integrated models were then constructed by combining the qualitative CT features and clinical features, respectively, using multivariate logistic regression with stepwise elimination.

Results: A total of 962 patients (aged, 61.7 ± 19.6 years; 490 men) were included; 179 (18.6%) were classified as severe/critical COVID-19, while 344 (35.8%) had a typical Radiological Society of North America (RSNA) COVID-19 appearance. The AUCs of the CT score models reached 0.91 (95% confidence interval (CI) 0.88–0.94), 0.82 (95% CI 0.76–0.87), and 0.83 (95% CI 0.77–0.89) during the early, intermediate, and late phases, respectively. The best cutoff values of the CT scores during each phase were 1.5, 4.5, and 5.5. The predictive accuracies associated with the time-dependent cutoff values reached 88% (vs.78%), 73% (vs. 63%), and 87% (vs. 57%), which were greater than those associated with universal cutoff value (all $P < 0.001$). The radiology score models reached AUCs of 0.96 (95% CI 0.94–0.98), 0.90 (95% CI 0.87–0.94), and 0.89 (95% CI 0.84–0.94) during the early, intermediate, and late phases, respectively. The integrated models including demographic and clinical risk factors greatly enhanced the AUC during the intermediate and late phases compared with the values obtained with the radiology score models; however, an improvement in accuracy was not observed.

Conclusion: The time interval between symptom onset and CT examination should be tracked to determine the cutoff value for the CT score for identifying severe/critical COVID-19. The radiology score combining qualitative CT features and the CT score complements clinical factors for identifying severe/critical COVID-19 patients and facilitates timely hierarchical diagnoses and treatment.

1. Introduction

Infectious diseases, such as coronavirus disease 2019 (COVID-19), threaten human life and can rapidly deplete and strain medical resources. Notably, COVID-19 exacerbated the shortage of medical resources in underdeveloped countries and has caused approximately seven million deaths worldwide over the past 3 years [1]. Although the World Health Organization (WHO) announced the end of the COVID-19 public health emergency in May 2023 [1], intermittent community transmission of this disease continues.

Chest computed tomography (CT) imaging is useful for diagnosing COVID-19 and is an important complement to nucleic acid tests when a patient first visits the hospital [2]. Several CT manifestations, including linear opacity, crazy-paving patterns, the involvement of upper lobes, air-bronchogram, and bronchial wall thickening, are associated with severe or critical COVID-19 [3–5]. Yang et al. [6] proposed a chest CT severity score in 2020 for quickly evaluating the severity of pulmonary involvement in patients with COVID-19, and a higher score was associated with a higher risk of poor hospital outcomes, such as intensive care unit (ICU) admission, mechanical ventilation (MVT), and death [6–9]. Nonetheless, these findings were mostly derived from CT scans of patients infected with previous strains. Recent studies have shown unique characteristics resulting from infection with the Omicron variant versus the Delta variant; for example, a lower incidence of typical COVID-19 CT findings, a reduced chest CT severity score, and an improved hospital outcome [10,11]. Therefore, the CT characteristics associated with severe or critical cases after infection with the emerging Omicron strains require additional investigation.

Many studies have shown the promising performance of CT scores for evaluating the disease severity and predicting the short-term prognosis of COVID-19 patients. For example, Yang et al. proposed using a CT severity score (0–2 points for 20 lung regions) to quickly and objectively evaluate the severity of pulmonary involvement in patients with COVID-19, and obtained an area under the curve (AUC) of 0.89 [6]. Other studies have shown that the CT score is correlated with 30-day mortality independent of age, respiratory rate, oxygen saturation levels, and comorbidities [8,12]. Elmokadem et al. examined different CT scoring systems for COVID-19 and reported very good-to-excellent (maximum AUC of 0.90) performance in detecting severe cases, and the results exhibited excellent interobserver agreement [13]. However, there remains a lack of standardized approaches for CT score use in real clinical settings, and the optimal cutoff values for CT scores vary [4,6,8]. One issue that previous studies have mostly overlooked is that the infection duration can greatly affect the CT findings associated with COVID-19 [8,14–16]. For example, Francone et al. [8] reported that a higher CT score is detected during the late phase (>7 days since symptom onset) of COVID-19 than during the early phase (≤7 days). Bernheim et al. [14] reported that consolidation and bilateral and peripheral disease are more common during the late phase (6–12 days since symptom onset) than during the early phase (0–2 days). Thus, the time interval between symptom onset and the first CT examination should be considered to determine the best cutoff value for the CT score for differentiating mild/moderate infection from severe/critical infection. Additionally, as clinical factors associated with COVID-19 severity have been well established [17,18], evaluating the imaging characteristics of COVID-19 patients alone may be insufficient.

Therefore, in this retrospective study, we sought to develop (1) a time-dependent model using the visualized CT score to identify severe/critical COVID-19 pneumonia and (2) an integrated model using the CT score, qualitative radiological features, demographic features, and clinical risk factors for the timely identification of severe/critical COVID-19 upon a patient's first visit to the hospital to facilitate hierarchical diagnosis and treatment.

2. Materials and methods

The institutional review board of our hospital approved this retrospective study (I-23PJ175), and the requirement for informed consent was waived.

2.1. Study design and population

Since the Chinese government loosened the national dynamic "zero-COVID" policy in November 2022, Beijing has witnessed the unprecedented impact caused by Omicron variants on medical services [19–21]. This retrospective study reviewed all consecutive patients who visited the fever clinic at our hospital from November 28, 2022, to January 8, 2023, during the peak Omicron outbreak. Following hospital protocol at that time, the fever clinic screened for COVID-19 infection and received all outpatients or emergency patients who had body temperatures over 37.3 °C or had suspected COVID-19. The inclusion criteria for our study were as follows: 1) a diagnosis of COVID-19 by positive real-time polymerase chain reaction detection of severe acute respiratory syndrome coronavirus 2 (SARS-CoV-2) nucleic acid or a positive antigenic test; and 2) the availability of chest CT scans on the same day as the first visit to our hospital. The exclusion criteria were as follows: 1) duration from symptom onset to CT scan exceeding 14 days; 2) interval between the CT scan and presentation at the hospital exceeding 24 h; 3) asymptomatic SARS-CoV-2 infection; 4) pregnancy; and 5) pediatric status (age <18 years).

The enrolled patients were divided into mild/moderate COVID-19 and severe/critical COVID-19 groups primarily according to their clinical symptoms and oxygenation status as described in the "Diagnosis and Treatment of Novel Coronavirus Infection (10th Trial Version)" published by China's National Health Commission in January 2023 (e-Appendix 1) [22]. The results were independently evaluated by a senior physician who specializes in respiratory diseases. The 30-day composite clinical outcomes, including the receipt of MVT or extracorporeal membrane oxygenation (ECMO), ICU admission, and in-hospital death, were extracted from the follow-up medical records.

2.2. Data collection and CT image acquisition

Demographic data (age, sex, smoking history, and vaccination status), preexisting comorbidities, clinical symptoms, initial laboratory findings, and clinical outcomes were extracted from the electronic medical records system. Vaccinated patients had received

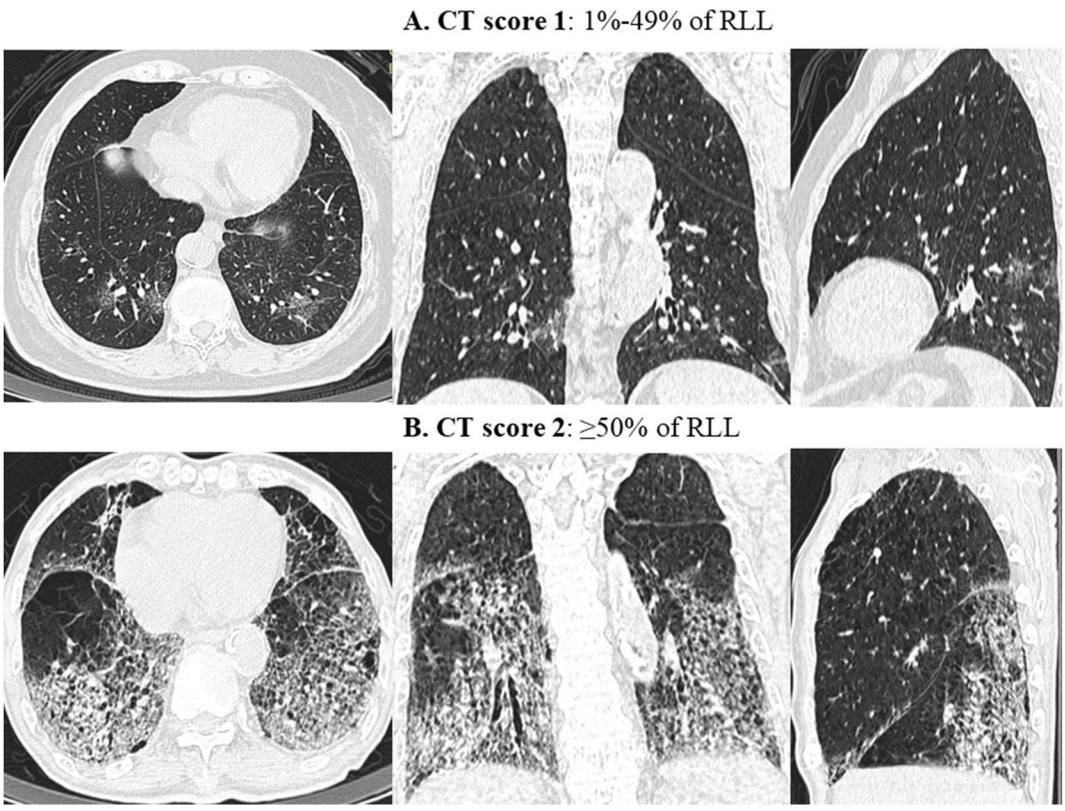

Fig. 1. Demonstration of different CT scores for the extent of RLL involvement in two COVID-19 patients on axial, coronal, and sagittal CT images of the lung window.

inactivated vaccines for COVID-19 (Sinovac-CoronaVac; Sinopharm, Beijing, China) during the mass vaccination campaign in the summer of 2021. Initial laboratory findings included the hemoglobin concentration, white blood cell count, lymphocyte count, platelet count, high-sensitivity C-reactive protein (hsCRP) level, and procalcitonin level. Thrombocytopenia was defined as a platelet count below 100×10^9/L. Anemia was defined as a hemoglobin level below 120 mg/dL. The predefined clinical thresholds for procalcitonin and high-sensitivity C-reactive protein elevation (hsCRP) were 0.5 ng/mL and 50 mg/L, respectively. The optimal thresholds for the neutrophil-to-lymphocyte ratio (NLR) and platelet-to-lymphocyte ratio (PLR) were determined to be 3.5 and 200, respectively, to maximize Youden's index during the receiver operating characteristic (ROC) curve analysis.

Chest CT scans were performed during a single inspiratory phase using an InsitumCT 768 from Sinovision (China) or an IQon Spectral CT from Philips Healthcare (the Netherlands) multi-detector CT scanners. All CT scans were obtained with the patient in the supine position during a single breath-hold. The tube voltage was 120 kV for all of the scans. Automatic exposure-control technology was used to adjust the tube current for each patient. All the images were reconstructed with slice thickness/interval values of 5 mm/5 mm, 1.25 mm/1.25 mm, or 1 mm/1 mm in the axial plane. The images were subsequently transmitted to the Picture Archiving and Communication System (Centricity PACS; GE Healthcare, Chicago, IL, USA) for further data analysis.

2.2.1. Image evaluation

Image analysis was performed using preselected lung (width, 1200 HU; level, −600 HU) and mediastinal (width, 450 HU; level, 50 HU) window settings. Two senior radiologists with 19 and 30 years of experience who were unaware of the patients' clinical and laboratory information reviewed the images separately and independently. Ambiguous findings were discussed to reach a conclusion by consensus. The extent of visualized pneumonia in each lobe on the CT scans was scored from 0 to 2 points (0 points, no evidence of pneumonia; 1 point, <50% involvement; and 2 points, ≥50% involvement) as proposed by Yang et al. [6] (Fig. 1). The CT score for the entire lung was the sum of the five lung lobe scores (0–10 points). Pneumonia patterns on the CT images were categorized per the RSNA Expert Consensus Statement [23]. The qualitative image features included previously reported prognostic factors for COVID-19 [7,24], such as pleural thickening, pleural effusion, pericardial effusion, lymph node enlargement, the "halo" sign, a "crazy paving" pattern, vacuole signs, bronchial distortion, bronchiectasis, bronchial wall thickening, air trapping, mucous plugs, and the "tree-in-bud" sign. Emphysema and interstitial lung disease were also evaluated according to typical CT findings and preexisting comorbidities. Pulmonary artery enlargement and aortic dilation were predefined as a main pulmonary artery diameter of >29 mm and an ascending aortic diameter of >34 mm, respectively, as revealed by CT [25,26].

2.3. Statistical analysis and sample size calculation

All analyses were performed using R (version 4.2.2; R Foundation for Statistical Computing, Vienna, Austria). A statistical assessment of the differences between groups was determined using the chi-square or Fisher's exact test (as appropriate) for categorical variables and the Wilcoxon rank-sum test for continuous variables. Multiple imputations ("mice" in R) were performed to handle the missing laboratory test results.

For the radiological feature analysis and model construction, the cohort was divided into three subcohorts depending on the duration from symptom onset to CT examination: early phase (0–3 days), intermediate phase (4–7 days), and late phase (8–14 days). In

Table 1
Group comparison of demographic characteristics and past medical history of patients with COVID-19.

Demographic and past medical history	All cohort	Mild/moderate	Severe/critical	*P*
Number of cases	962	783 (81.4)	179 (18.6)	
Sex (%)				**<0.001**
Male	490 (50.9)	371 (47.4)	119 (66.5)	
Female	472 (49.1)	412 (52.6)	60 (33.5)	
Age (mean (SD))	61.7 (19.6)	58.75 (19.39)	74.50 (14.53)	**<0.001**
Smoking history				**<0.001**
Never smoker	513 (53.3)	430 (54.9)	83 (46.5)	
Current smoker	16 (1.7)	10 (1.3)	6 (3.4)	
Ever smoker	28 (2.9)	14 (1.8)	14 (7.6)	
Missing	405 (42.1)	329 (42.0)	76 (42.5)	
Comorbidities	704 (73.2)	535 (68.3)	169 (94.4)	**<0.001**
Diabetes	203 (21.1)	141 (18.0)	62 (34.6)	**<0.001**
Cardiovascular disease	418 (43.5)	307 (39.2)	111 (62.0)	**<0.001**
Cerebrovascular disease	114 (11.9)	72 (9.2)	42 (23.5)	**<0.001**
Chronic lung disease	176 (18.3)	122 (15.6)	54 (30.2)	**<0.001**
Chronic liver or kidney disease	94 (9.8)	66 (8.4)	28 (15.6)	**0.005**
Immunocompromised status/malignancies	274 (28.5)	218 (27.8)	56 (31.3)	0.41
Vaccination status				0.34
Unvaccinated	104 (10.8)	80 (10.2)	24 (13.4)	
1–2 shots	63 (6.5)	52 (6.6)	11 (6.2)	
Booster shot	81 (8.4)	69 (8.8)	12 (6.7)	
Missing	714 (74.2)	582 (74.3)	132 (73.7)	

Note—Except where indicated, data are numbers of patients, with percentages in parentheses. Booster shot refers to the receipt of 3 or 4 shots.

each of the subcohorts, a multivariate regression analysis with stepwise backward elimination ("stepAIC" in R) was applied to establish the radiology score (CT score and qualitative CT features), the integrated model (radiology score and demographic features), and the integrated^{CRF} model (radiology score, demographic features, and clinical risk factors). A univariable logistic regression was used to evaluate the association between the CT/radiology scores and clinical outcomes. ROC analysis was then performed, and the AUC was compared using the Delong test. Time-dependent cutoff values and a universal cutoff value were determined to maximize Youden's index in each sub-cohort and the entire cohort separately, and the associated accuracies were compared using the McNemar test. A P value < 0.05 was considered to indicate a significant difference throughout the study. The sample sizes used for the predictive models were calculated as described by Riley et al. [27] and determined using the "pmsampsize" package in R with the following parameters: type = 'b', Rsquared = 0.199, parameters = 6, and prevalence = 0.19. The minimum sample size required for new model development with our settings was 241 cases with 46 events.

3. Results

3.1. Participation and baseline characteristics

A review of 1782 infected patients from the fever clinic was conducted. After excluding ineligible patients, 962 (mean age, 61.7 ± 19.6 years, 490 men) were included in our analysis. Severe/critical COVID-19 at presentation accounted for 18.6% (179/962) of the entire cohort. As summarized in Table 1, the severe/critical COVID-19 patients were more likely to be male, older, smokers, and to

Table 2
CT features of patients with pneumonia at different phases by clinical stage.

CT features	Entire cohort	Early phase (0-3 d)			Intermediate phase (4-7 d)			Late phase (8-14 d)		
	Severe/ critical	Mild/ moderate	Severe/ critical	*P*	Mild/ moderate	Severe/ critical	*p*	Mild/ moderate	Severe/ critical	*P*
N	179	310	51		292	68		181	60	
CT score (mean (SD))										
LUL	0.95 (0.6)	0.2 (0.4)	0.8 (0.6)	**<0.001**	0.5 (0.5)	0.9 (0.8)	**<0.001**	0.6 (0.5)	1.2 (0.5)	**<0.001**
LLL	1.27 (0.6)	0.3 (0.5)	1.3 (0.6)		0.6 (0.5)	1.2 (0.6)		0.7 (0.5)	1.3 (0.6)	
RUL	0.95 (0.6)	0.2 (0.4)	0.8 (0.6)		0.5 (0.5)	0.9 (0.6)		0.6 (0.5)	1.1 (0.6)	
RML	1.03 (0.7)	0.1 (0.3)	0.8 (0.7)		0.4 (0.5)	1.1 (0.7)		0.5 (0.5)	1.2 (0.6)	
RLL	1.2 (0.6)	0.3 (0.5)	1.1 (0.6)		0.6 (0.5)	1.3 (0.6)		0.8 (0.4)	1.3 (0.6)	
Total	5.4 (2.3)	0.95 (1.6)	4.7 (2.4)	**<0.001**	2.5 (2.1)	5.4 (2.3)	**<0.001**	3.2 (2.1)	6.1 (2.1)	**<0.001**
Lobe number (mean (SD))	4.2 (1.3)	0.9 (1.5)	3.8 (1.5)	**<0.001**	2.5 (2.0)	4.1 (1.4)	**<0.001**	3.1 (2.0)	4.6 (0.9)	**<0.001**
Pleural thickening	115 (64.2)	51 (16.5)	32 (62.7)	**<0.001**	64 (21.9)	42 (61.8)	**<0.001**	47 (26.0)	41 (68.3)	**<0.001**
Pleural effusion	97 (54.2)	35 (11.3)	32 (62.7)	**<0.001**	39 (13.4)	35 (51.5)	**<0.001**	22 (12.2)	30 (50.0)	**<0.001**
Pericardial effusion	64 (35.8)	36 (11.6)	22 (43.1)	**<0.001**	33 (11.3)	26 (38.2)	**<0.001**	28 (15.5)	16 (26.7)	0.18
Lymph node enlargement	31 (17.3)	4 (1.3)	9 (17.6)	**<0.001**	12 (4.1)	12 (17.6)	**<0.001**	17 (9.4)	10 (16.7)	0.37
Halo sign	20 (11.2)	3 (1.0)	7 (13.7)	**<0.001**	25 (8.6)	9 (13.2)	0.25	23 (12.7)	4 (6.7)	0.24
Crazy-pavement	48 (26.8)	10 (3.2)	6 (11.8)	**0.02**	56 (19.2)	18 (26.5)	0.19	56 (30.9)	24 (40.0)	0.21
Vacuole sign	54 (30.2)	13 (4.2)	10 (19.6)	**<0.001**	62 (21.2)	22 (32.4)	0.06	58 (32.0)	22 (36.7)	0.53
Bronchial distortion	107 (59.8)	21 (6.8)	27 (52.9)	**<0.001**	46 (15.8)	42 (61.8)	**<0.001**	43 (23.8)	38 (63.3)	**<0.001**
Bronchiectasis	109 (60.9)	16 (5.2)	20 (39.2)	**<0.001**	61 (20.9)	47 (69.1)	**<0.001**	55 (30.4)	42 (70.0)	**<0.001**
Bronchial wall thickening	147 (82.1)	84 (27.1)	44 (86.3)	**<0.001**	111 (38.0)	59 (86.8)	**<0.001**	77 (42.5)	44 (73.3)	**<0.001**
Air trapping	56 (31.3)	47 (15.2)	21 (41.2)	**<0.001**	42 (14.4)	21 (30.9)	**0.002**	22 (12.2)	14 (23.3)	0.06
Mucous plugging	27 (15.1)	15 (4.8)	12 (23.5)	**<0.001**	21 (7.2)	8 (11.8)	**0.22**	5 (2.8)	7 (11.7)	**0.012**
Tree-in-bud nodularity	19 (10.6)	22 (7.1)	10 (19.6)	**0.007**	38 (13.0)	8 (11.8)	>0.99	8 (4.4)	1 (1.7)	0.46
Aortic dilation	104 (58.1)	61 (19.7)	35 (68.6)	**<0.001**	107 (36.6)	41 (60.3)	**0.001**	87 (48.1)	28 (46.7)	0.88
Pulmonary artery enlargement	64 (35.8)	37 (11.9)	20 (39.2)	**<0.001**	35 (12.0)	24 (35.3)	**<0.001**	22 (12.2)	20 (33.3)	**0.001**
Emphysema	55 (30.7)	25 (8.1)	16 (31.4)	**<0.001**	36 (12.3)	22 (32.4)	**<0.001**	33 (18.2)	17 (28.3)	0.101
Interstitial lung disease	23 (12.8)	23 (7.4)	5 (9.8)	0.57	12 (4.1)	12 (17.6)	**<0.001**	12 (6.6)	6 (10.0)	0.401

Note—Except where indicated, data are numbers of patients, with percentages in parentheses. Percentages were calculated by dividing the current number by the number of n within the same column. For example, pleural thickening was present in 51 patients in the mild/moderate group in the early phase and the percentage was calculated as 51/310 = 16.5%. *P* values were calculated for the difference of variable between groups unless otherwise indicated.

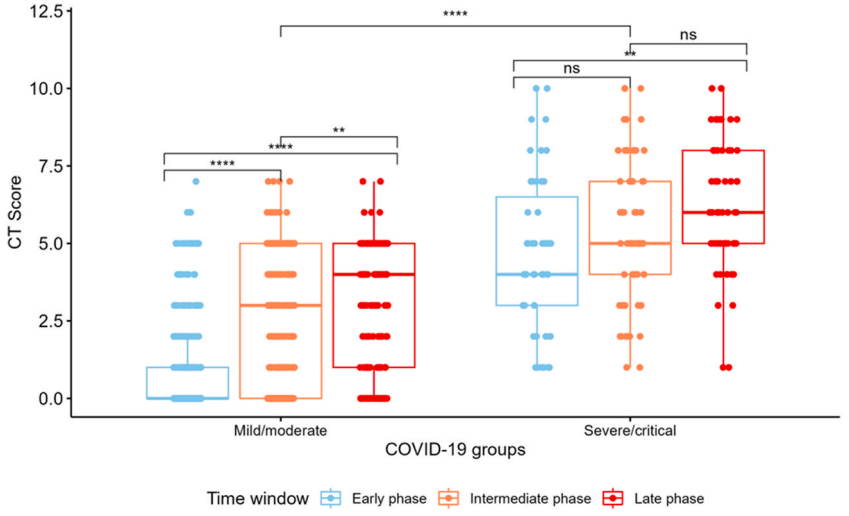

Fig. 2. Box-and-whisker plots showing CT scores according to time phase for the mild/moderate and severe/critical groups. *: $P < .05$; **: $P < .01$; ***: $P < .001$; ****: $P < .0001$; ns: no statistical significance.

have at least one preexisting comorbidity. As shown in e-Table 1, the severe/critical COVID-19 group exhibited significantly higher incidences of fever lasting over five days (45.8%), chest tightness (57.5%), drowsiness (15.6%), and cognitive disorders (14.5%), while the mild/moderate COVID-19 group exhibited higher incidences of myalgia (22.6%) and chills (27.2%). Increased white blood cell and neutrophil counts, decreased lymphocyte and eosinophil counts, elevated NLR, hsCRP, and procalcitonin were more prevalent in the severe/critical COVID-19 group than in the mild/moderate COVID-19 group ($P < 0.001$) (e-Table 2). The association between age and COVID-19 severity is shown in e-Fig. 1. The percentage of severe/critical COVID-19 was lower in the booster vaccination group (6% nonelderly individuals; 27% elderly individuals) than in the unvaccinated group (vs. 11%, $P = 0.69$; vs. 30%, $P = 0.79$), regardless of age (e-Fig. 2).

According to the RSNA COVID-19 classification, a typical appearance was noted in 35.8% (344/962) of the patients, and an indeterminate appearance was noted in 22.8% (219/962). The dynamic change in the proportion of patients in each COVID-19 classification is illustrated in e-Fig. 3.

3.2. *Time-dependent chest CT scores and qualitative features of severe/critical COVID-19 patients*

As shown in Table 2, compared to the mild/moderate COVID-19 group (0.95 ± 1.6, early phase; 2.5 ± 2.1, intermediate phase; 3.2 ± 2.1, late phase), the severe/critical COVID-19 group had higher CT scores (vs. 4.7 ± 2.4, $P < 0.001$; 5.4 ± 2.3, $P < 0.001$; 6.1 ± 2.1, $P < 0.001$) across the study period. As the interval between the CT scan and symptom onset increased, the CT scores increased significantly in both the mild/moderate COVID-19 and severe/critical COVID-19 groups (Fig. 2). In addition, the significant difference in the total CT score between the lower lobes and upper lobes observed during the early stage of COVID-19 gradually disappeared over time (Fig. 3).

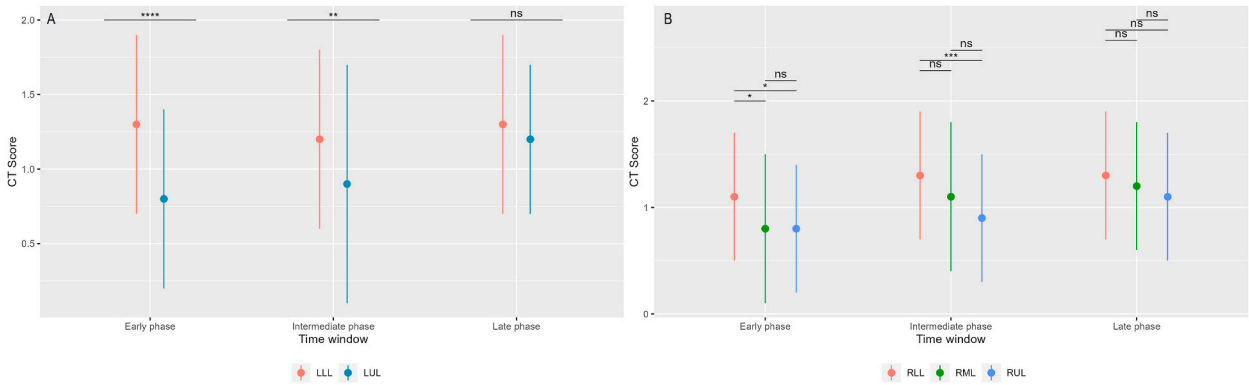

Fig. 3. CT scores of the individual lobes in the severe/critical group. (A) Represents the left lobe and (B) represents the right lobe. Abbreviations: LLL, left lower lobe; LUL, left upper lobe; RUL, right upper lobe; RML, right middle lobe; RLL, right lower lobe. *: $P < .05$; **: $P < .01$; ***: $P < .001$; ****: $P < .0001$; ns: not significant.

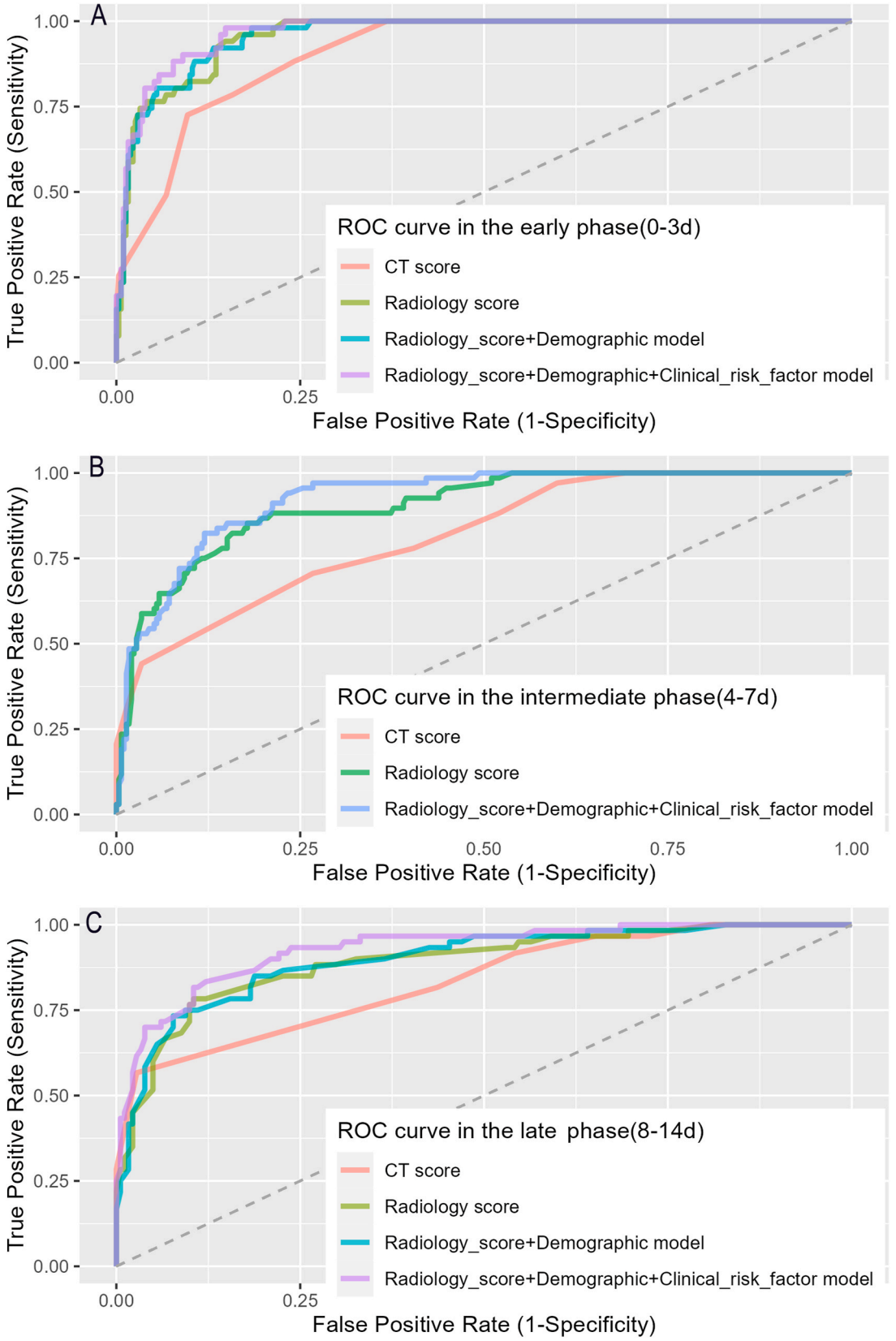

(caption on next page)

Fig. 4. Receiver operating characteristic curves of CT score, radiology score, radiology score + demographic model (integrated model), and radiology score + demographic + clinical risk factors model (integrated^{CRF} model) for identifying severe/critical COVID-19 in the early phase (A), intermediate phase (B), and late phase (C).
Note: Radiology score+demographic model does not exist in the intermediate phase and was not shown in the figure on purpose.

The incidence of pleural effusion was 18.6% (67 of 361) for patients in the early disease phase. Distinctive CT features that were more prevalent in the severe/critical group in the early-to-intermediate phase included pericardial effusion, lymph node enlargement, aortic dilation, and emphysema. The halo sign, crazy-paving pattern, vacuole sign, and tree-in-bud nodularity were significantly more frequent in the severe/critical COVID-19 patients only during the early phase. The distributions of the remaining qualitative CT characteristics are shown in Table 2.

3.3. CT score-based model for identifying severe/critical COVID-19

The ROC analysis (Fig. 4) revealed that the AUCs of the CT scores reached 0.91 [0.88–0.94], 0.82 [0.76–0.87], and 0.83 [0.77–0.89] during the early, intermediate, and late phases, respectively. The optimal cutoff values of the CT scores to maximize the ROC curve Youden index were 1.5, 4.5, and 5.5 during the early, intermediate, and late phases, respectively. Once the calculated score surpassed the corresponding threshold, the patient was classified as a severe/critical case. Compared to that using the universal cutoff value (3.6), the accuracy of the model using the time-dependent cutoff values significantly increased from 78% to 88% (McNemar test, $P < 0.001$), 63% to 73% (McNemar test, $P < 0.001$), and 57% to 87% (McNemar test, $P < 0.001$).

The radiology models used during the three phases consisted of the CT score, pleural effusion, pericardial effusion, emphysema, bronchial distortion, air trapping, and crazy-paving patterns during the early phase; the CT score, pleural thickening, pleural effusion, emphysema, bronchial distortion, and bronchial wall thickening during the intermediate phase; and the CT score, pleural thickening, pleural effusion, and pulmonary artery enlargement during the late phase (Table 3). The ROC analysis (Fig. 4) revealed that the AUCs of the radiology scores were significantly greater than those of the CT scores alone ($P < 0.05$ for all), reaching 0.96 [0.94–0.98], 0.90 [0.87–0.94], and 0.89 [0.84–0.94] during each of the sequential phases. As shown in Fig. 5, the radiology scores during each phase were calculated by combining the abovementioned features with linear polynomial equations. Fewer areas overlapped between the density curves of the radiology scores between the mild/moderate and severe/critical COVID-19 groups than between the density curves of the CT scores across all phases (Fig. 6).

3.4. Multivariate analysis of the CT scores, radiology scores, and clinical features

The multivariate analysis results (e-Table 3) revealed an increased risk for severe/critical COVID-19 when a higher radiology score is present during the early (adjusted odds ratio (OR) 3.0, 95% CI 2.1–4.3, $P < 0.001$), intermediate (adjusted OR 2.4, 95% CI 1.8–3.2, $P < 0.001$), and late (adjusted OR 2.4, 95% CI 1.7–3.4, $P < 0.001$) phases.

The demographic features included sex and age. Clinical risk factors included comorbidities, a high white blood cell count, a high NLR, a low eosinophil count, and a high hsCRP level. Smoking status, vaccination status, and procalcitonin levels were not included due to a large proportion of missing values. When combining the radiology scores with preexisting comorbidities and the hsCRP, the AUC of the integrated^{CRF} model was significantly greater (from 0.90 to 0.93, $P = 0.024$) during the intermediate phase. During the late phase, the integrated^{CRF} model that combined the radiology score, age, preexisting comorbidities, and the NLR significantly enhanced the AUC of the predictive model (from 0.89 to 0.93, $P = 0.008$) (Table 4). Nonetheless, the prediction accuracy did not improve and even decreased during the intermediate phase (from 83% to 80%). The performances of the models that combined the CT scores and clinical features are shown in e-Tables 4 and 5 in the supplementary material.

3.5. Relationship between the 30-day composite clinical outcomes and the radiology score

Among the 195 patients with known 30-day clinical outcomes, 31.8% (62/195) had experienced composite adverse outcomes (eight died, 31 required MVT or ECMO, and 23 were admitted to the ICU). E-Table 6 illustrates that an increased risk of experiencing adverse clinical outcomes is associated with a higher radiology score (adjusted OR for death, 1.8; 95% CI, 1.1–2.8; $P = 0.01$; MVT/ECMO, 2.0; 1.5–2.6; $P < 0.001$; ICU admission, 1.3; 1.0–1.7; $P = 0.06$). Significant differences in the CT scores between the early and intermediate phases and between the early and late phases were observed in patients without adverse events (Fig. 7). In patients with composite adverse clinical outcomes, the total CT score was relatively lower during the early phase than during the later phases, although significance was not reached. No evidence of a difference between the total CT scores during the intermediate and late phases was observed.

4. Discussion

The high transmission rate of the COVID-19 variant poses significant challenges for the clinical management of COVID-19 patients. In this study, we found that the percentage of severe and critical COVID-19 patients at presentation was 18.6%, which increased with age regardless of preexisting comorbidities. The optimal cutoff values for the CT score for differentiating severe/critical COVID-19 and mild/moderate COVID-19 were 1.5 during the early phase and 5.5 during the late phase. Pleural effusion was observed in 18.6% of

Table 3
Multivariate logistic model determining the radiology score in three subcohorts across three phases.

Multivariable analysis	**Early phase** (0–3 days from symptom onset)			**Intermediate phase** (4-7days from symptom onset)			**Late phase** (8–14 days from symptom onset)		
Characteristics	**OR**	**95%CI**	***P***	**OR**	**95%CI**	***P***	**OR**	**95%CI**	***P***
CT score	1.99	1.59–2.51	**<0.001**	1.73	1.4–2.15	**<0.001**	2.06	1.54–2.75	**<0.001**
Pleural thickening	/	/	/	2.02	0.99–4.12	0.05	2.31	1.02–5.2	**0.04**
Pleural effusion	6.71	2.68–16.82	**<0.001**	3.25	1.56–6.75	**<0.001**	4.81	2.07–11.19	**<0.001**
Pericardial effusion	2.45	0.95–6.35	0.07	/	/	/	/	/	/
Emphysema	4.55	1.49–13.86	**0.01**	2.75	1.24–6.09	**0.01**	/	/	/
Bronchial distortion	3.56	1.33–9.53	**0.01**	1.85	0.9–3.81	0.1	/	/	/
Bronchial wall thickening	/	/	/	3.66	1.52–8.83	**<0.001**	/	/	/
Air trapping	2.75	1.06–7.1	**0.04**	/	/	/	/	/	/
Crazy-pavement	0.2	0.04–0.94	**0.04**	/	/	/	/	/	/
Pulmonary artery enlargement	/	/	/	/	/	/	2.19	0.84–5.7	0.11
Radiology score formula	−5.43 + 0.69 × CT_score +1.9 × Pleural_effusion+0.89 × Pericardial_effusion+1.51 × Emphysema +1.27 × Bronchial_distortion −1.62 × Crazy-pavement+1.01 × Air_trapping			−5.78 + 0.55 × CT_score +0.7 × Pleural_thickening+1.18 × Pleural_effusion+1.01 × Emphysema +0.61 × Bronchial_distortion +1.3 × Bronchial_wall_thickening			−5.58 + 0.72 × CT_score +0.84 × Pleural_thickening+1.57 × Pleural_effusion+0.79 × Pulmonary_artery_enlargement		
Integrated **model formula**	0.45 + 1.01 × radiology_score-1.05 × Female			Demographic features were not selected in the final model.			−0.66 + 0.98 × radiology_score+ 0.89 × Elder		
Integrated^{CRF} model formula	0.22 + 1.13 × radiology_score −0.91 × Female-1.21 × Comorbidities*+1.74 × high_NLR$			−2.02 + 0.88 × radiology_score +1.14 × Comorbidities*+1.44 × high_hsCRP#			−4.17 + 0.84 × radiology_score +0.92 × Elder+1.43 × Comorbidities*+2.56 × high_NLR$		

Abbreviations: OR = odds ratio, CI = confidence interval, NLR = neutrophil-to-lymphocyte ratio, hsCRP = high-sensitivity C-reactive protein. Categorical variables were attributed to value 1 as indicated. *: The existence of any of the following comorbidities: diabetes, cardiovascular disease, cerebrovascular disease, chronic lung disease, cardiovascular disease and immunocompromised status or malignancies. $: High NLR was defined as the ratio of neutrophil count and lymphocyte count was above 3.5. #f: High hsCRP was defined as hsCRP>50 mg/L. Integrated model was consisted of radiology score and demographic feature. Integrated^{CRF} model was consisted of radiology score, demographic feature, and clinical risk factors.

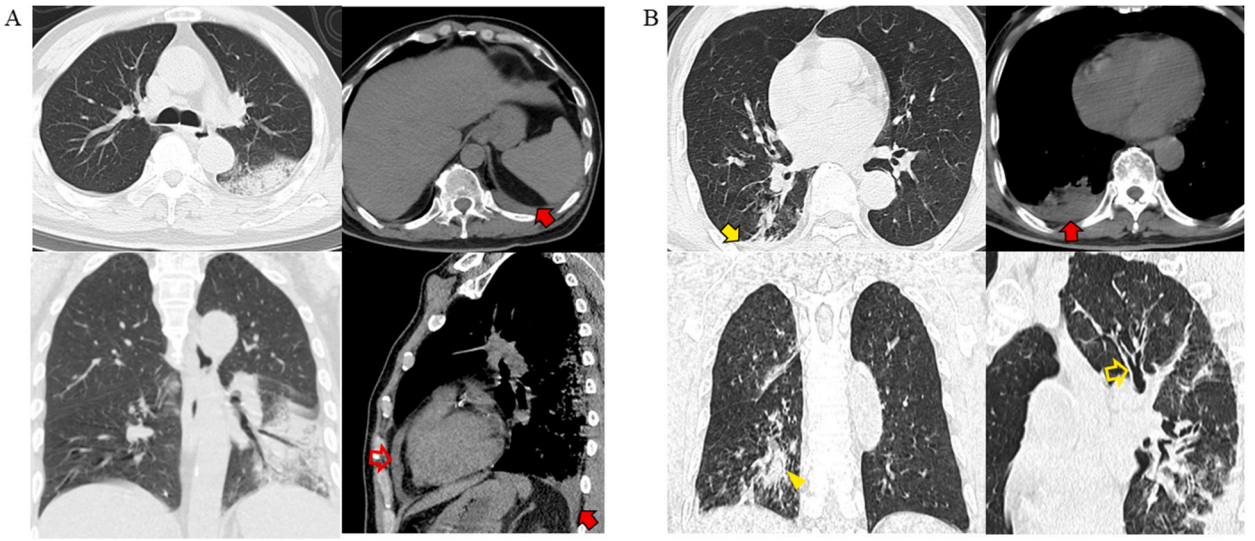

Fig. 5. Illustration of different radiology scores of the whole lung in two COVID-19 patients. (A): Early phase, clinical type = severe pneumonia, total CT score = 2, pleural effusion = 1 (red solid arrow), pericardial effusion = 1 (red hollow arrow), emphysema = 0, bronchial distortion = 0, crazy paving patterns = 0, air trapping = 0; Radiology score = -5.43 + 0.69 × 2 + 1.9 × 1 + 0.89 × 1 + 1.51 × 0 + 1.27 × 0 – 1.62 × 0 + 1.01 × 0 = −1.26 (>-2.3) classification correct. (B): Intermediate phase, clinical type = severe pneumonia, total CT score = 3, pleural thickening = 1 (yellow solid arrow), pleural effusion = 1 (red arrow), emphysema = 0, bronchial distortion = 1 (yellow arrowhead), bronchial wall thickening = 1 (yellow hollow arrow); Radiology score = −5.78 + 0.55 × 3 + 0.7 × 1 + 1.18 × 1 + 1.01 × 0 + 0.61 × 1 + 1.3 × 1 = −0.34 (>-1.5), correct classification.

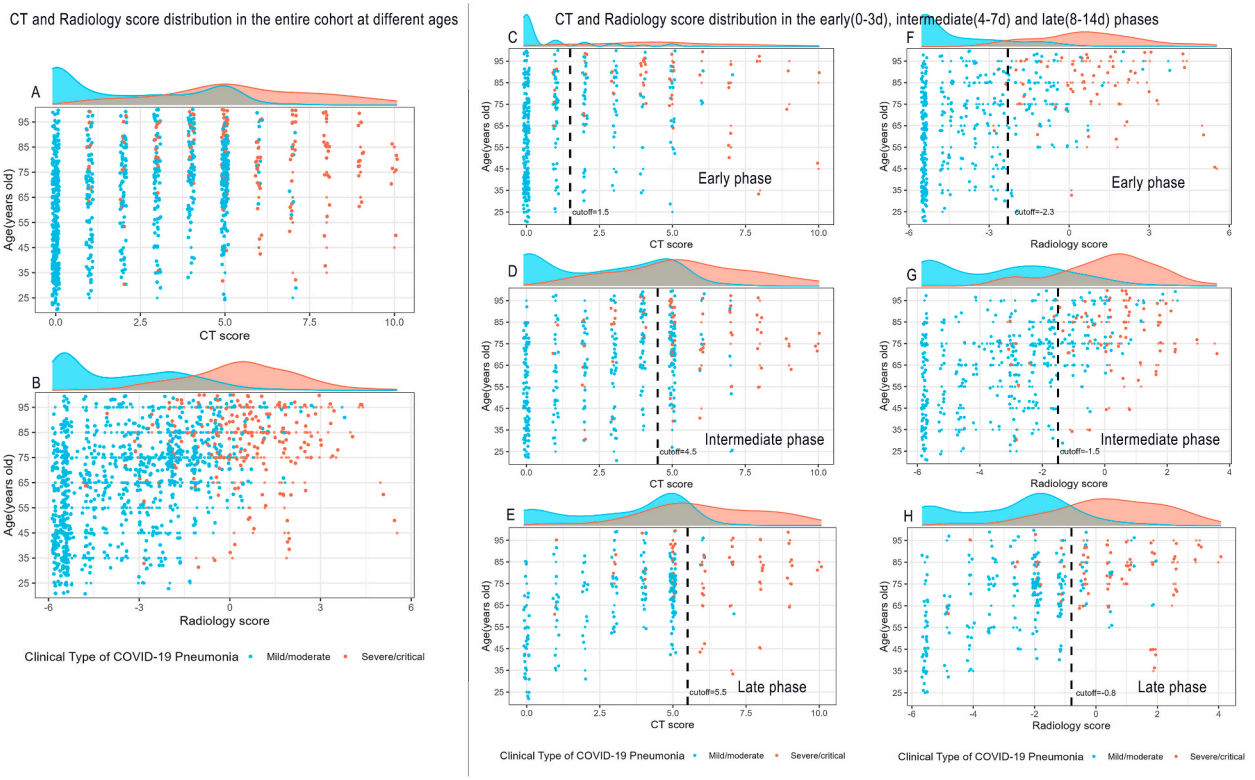

Fig. 6. CT and radiology scores of the entire cohort (n = 962). The left panel shows the relationship between age and CT score (A) or radiology score (B). Each dot represents one patient. Light blue denotes the mild/moderate type of COVID-19, and coral denotes the severe/critical type. The density curves on the top axis of each plot reflect the distribution of different clinical types of COVID-19. C–E: Correlations among CT score, age, and clinical type of COVID-19 in the early phase (C), intermediate phase (D), and late phase (E). F–H: Correlations among the radiology score, age, and clinical type of COVID-19 in the early phase (F), intermediate phase(G), and late phase (H).

Table 4
Parameters of ROC curves of CT score, radiology score, integrated model, and integrated^{CRF} model.

Characteristics	Early phase (0–3 days from symptom onset)								
	Cutoff	AUC (95%CI)	Accuracy (95%CI)	Sensitivity	Specificity	PPV	NPV	*P1* (AUC)	*P2* (AUC)
CT score	1.5	0.91 (0.88–0.94)	88% (84%–91%)	88%	76%	38%	98%	Ref.	/
CT score*	3.6	0.91 (0.88–0.94)	78% (73%–82%)	73%	90%	55%	95%	/	/
Radiology score	−2.3	0.96 (0.94–0.98)	85% (81%–89%)	96%	83%	49%	99%	**<0.001**	Ref.
Integrated model	0.52	0.96 (0.94–0.98)	84% (80%–88%)	98%	82%	47%	100%	**<0.001**	0.896
Integrated^{CRF} model	0.52	0.97 (0.95–0.98)	87% (83%–90%)	98%	85%	52%	100%	**<0.001**	0.497
Intermediate phase (4–7 days from symptom onset)									
CT score	4.5	0.82 (0.76–0.87)	73% (68%–77%)	71%	73%	38%	91%	Ref.	/
CT score*	3.6	0.82 (0.76–0.87)	63% (58%–68%)	78%	60%	31%	92%	/	/
Radiology score	−1.5	0.90 (0.87–0.94)	83% (78%–87%)	85%	82%	53%	96%	**<0.001**	Ref.
Integrated model	**Demographic features were not selected in the final model.**								
Integrated^{CRF} model	0.53	0.93 (0.90–0.95)	80% (75%–84%)	94%	77%	48%	98%	**<0.001**	**0.024**
Late phase (8–14 days from symptom onset)									
CT score	5.5	0.83 (0.77–0.89)	87% (82%–91%)	57%	97%	87%	87%	Ref.	/
CT score*	3.6	0.83 (0.77–0.89)	57% (51%–64%)	92%	46%	36%	94%	/	/
Radiology score	−0.8	0.89 (0.84–0.94)	87% (82%–91%)	78%	90%	71%	93%	**0.005**	Ref.
Integrated model	0.54	0.90 (0.85–0.94)	82% (77%–87%)	85%	81%	60%	94%	**0.004**	0.442
Integrated^{CRF} model	0.57	0.93 (0.89–0.97)	87% (82%–91%)	83%	88%	69%	94%	**<0.001**	**0.008**

Abbreviations: AUC, area under the curve; PPV, positive predictive value; NPV, negative predictive value; CI, confidence interval. *: Without considering the time window, the optimal cutoff of total CT score was 3.6 if all patients were combined to build the model. Radiology score was consisted of total CT score and qualitative CT characteristics. Integrated model was consisted of radiology score and demographic feature. Integrated^{CRF} model was consisted of radiology score, demographic feature, and clinical risk factors.

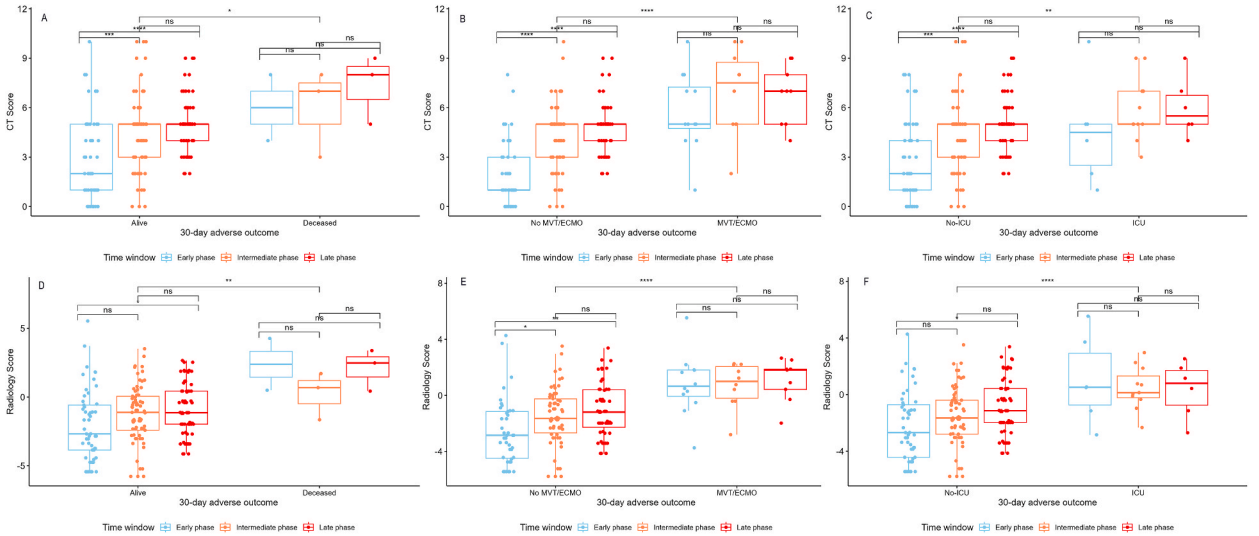

Fig. 7. Box-and-whisker plots of the CT score (A–C) and radiology score (D–F) by time phases for 30-day composite clinical outcomes. The data are shown from left to right as follows: alive vs. deceased (A, D), mechanical ventilation (MVT)/ECMO vs. no MVT/ECMO (B, E), and admission to intensive care unit (ICU) vs. no ICU (C, F). The bar in the box represents the median. The upper and lower limits of the whiskers indicate 1.5 times the interquartile range above and below the upper and lower quartiles, respectively, and the dots indicate each patient. *: $P < .05$; **: $P < .01$; ***: $P < .001$; ****: $P < .0001$; ns: no statistical significance.

patients in the early phase. Additionally, lymph node enlargement, pericardial effusion, a halo sign, a vacuole sign, and tree-in-bud nodularity were significantly more common in the severe/critical patients during the early phase but gradually decreased during later phases. The radiology score combined with the CT score and qualitative radiological features exhibited excellent performance in identifying severe/critical COVID-19 during all three phases and was also associated with an increased risk for requiring MVT or ECMO. The demographic features and clinical risk factors enhanced the AUC of the radiology score during the intermediate phase and late phase, but the accuracy of the models did not significantly improve.

Although reduced hospitalization rates and severity degrees of CT pneumonia associated with Omicron strains compared to Delta strains have been noted, our study documented substantially greater rates of severe/critical COVID-19 at presentation to the hospital and worse 30-day composite clinical outcomes than previous Omicron studies [28,29]. Rates of 18.6% for severe/critical COVID-19 and 31.8% for 30-day adverse clinical outcomes were found in our study, whereas only 5% of severe/critical COVID-19 patients

developed pneumonia in a large cohort study performed by Lu et al. [30] on patients in Shanghai, China. In addition, Lee et al.'s [28] study of patients in Korea indicated that 14% (12 of 88) reached the 30-day composite outcome. Tsakok et al. [10] found that, upon hospitalization for Omicron infection, only 2% (vs. 11.8% in our study) of patients required critical care. These contradictory findings might be attributable to several factors. First, patients with mild symptoms might choose not to undergo chest CT imaging upon presentation to the hospital, leading to a selection bias. Second, most patients in our study had no prior exposure to SARS-CoV-2, and their vaccination interval potentially exceeded the protection time window, increasing their vulnerability to the current variants. Third, the enhanced neutralization resistance and replicative kinetics of BA.5.2 and BF.7 further weakened their immune protection [31,32]. Despite these limitations, our study highlights the enormous pressure that a tertiary hospital in China faced during the Omicron wave and the need for the timely identification and management of severe/critical COVID-19 cases [33].

Although pleural effusion has been regarded as a risk factor for ICU admission and mortality in previous studies, the reported incidence is generally less than 10% in the early phase [7,34]. However, we found that the incidence of pleural effusion associated with Omicron infection reached 18.6% (67 of 361) in the early phase. This difference may be explained by the older age and greater incidence of comorbidities, especially cardiovascular diseases, in our cohort. In addition, several distinctive CT features of severe/-critical COVID-19 at an early disease stage were identified. Lymph node enlargement and pericardial effusion correlate with an acute inflammatory response and are reportedly associated with increased mortality and prolonged hospitalization in COVID-19 patients [15,35]. The vacuole sign is caused by dilation of the alveolar duct and sac and indicates alveolar destruction and the potential development of fibrosis [36]. Notably, the incidences of the tree-in-bud and halo signs ranged from 10 to 20% in the severe/critical group in the early phase, while the incidences decreased significantly in the late phase. The halo sign is consisted of the peripheral ground-glass opacity and the central consolidation zone. Previous studies have indicated that the incidence of the halo sign nears 34%; however, few have demonstrated a correlation between COVID-19 severity and the halo sign [37]. It is suggested that the ground-glass opacity results from extensive damage to the pulmonary microcirculation, which can induce fibrosis in the later phase [38]. The tree-in-bud sign is an atypical CT characteristic of COVID-19 with an incidence of approximately 4% [37]; however, we demonstrated an occurrence of 19.6% among severe/critical COVID-19 patients in the early phase. The tree-in-bud sign indicates bronchiolar luminal impaction with mucus, pus, or fluid and is nonspecific for SARS-CoV-2 infection. Its early presence implies pathogen spread within airways or coinfection with other pathogens.

The mean CT score of severe and critical patients was significantly lower during the early phase than during the intermediate and late phases. Previous studies have developed different thresholds for total CT scores to identify severe or critical COVID-19 patients, but none have considered the impact of the interval between symptom onset and the initial CT examination [3,6,8]. Additionally, our study revealed a waning difference in the CT score between different lobes as time elapsed after symptom onset, underscoring the importance of tracking the time since symptom onset to accurately identify patients with severe/critical COVID-19 pneumonia.

Moreover, by combining the total CT score with qualitative CT features, we developed a radiology score with a significantly greater AUC than that of the CT score alone, especially for the intermediate phase. The addition of qualitative evaluations to increase the performance of the predictive models is not new [4,39]. Features such as emphysema represent preexisting chronic lung diseases that may render patients vulnerable to viral attacks [40,41]. Bronchial distortion and bronchial wall thickening can reflect ongoing or past fibrotic changes that signal a comorbid factor that precipitates the development of severe/critical pneumonia [42]. This difference might also be attributable to diffuse alveolar damage during the acute/subacute disease stage.

This study had some limitations. First, this was a retrospective study of data from a single center in Beijing during a specific time window, and the patients tended to be older and were more likely to have preexisting comorbidities. In the future, multicenter data from a larger age spectrum should be used to validate the proposed models. Second, a comparison of the CT features between the studied strains and previous strains was not conducted because we could not access the data from the previous strains. Third, we did not have the exact date of vaccination for each patient, which could have affected the vaccine efficacy analysis. Fourth, information regarding smoking history, prior infection history, and medication history was mostly unavailable due to the study's retrospective nature. Nonetheless, our findings indicate that the CT score is a relatively independent index that reflects the overall health condition of the lung. Future studies could assess the correlation between the CT score and the abovementioned clinical factors. Finally, the CT characteristics of our study were based on two specific Omicron strains circulating during the Beijing pandemic in November 2022 and January 2023, and whether these findings apply to the forthcoming strains remain unknown. Nonetheless, our findings suggest a correlation between infection duration and the CT score that is not restricted to these two specific strains.

In summary, in this study we constructed three CT score-based models for three different disease phases to accurately identify severe/critical COVID-19. In addition, the study revealed that the best cutoff values of the CT score for identifying severe/critical COVID-19 pneumonia are associated with the interval between symptom onset and CT examination. We envision that such an approach could be applied to local health emergencies caused by new variants of SARS-CoV-2 and other acute infectious diseases.

Ethical approval

The study and the request for a waiver of informed consent were approved by the institutional review board of Peking Union Medical College Hospital (I-23PJ175). This retrospective study was conducted using documented and anonymous clinical data and information and did not involve personal privacy or commercial interests. The waiver of informed consent will not adversely affect the rights and interests of the subjects.

Funding statement

This study has received funding from the National Science and Technology Major Project (No. 2021ZD0111105), the National Natural Science Foundation of China (NSFC No. 82171934), and the Beijing Municipal Key Clinical Specialty Excellence Program. The funders had no role in the study design, data collection and analysis, decision to publish, or preparation of the manuscript.

Data availability statement

Data will be made available on request.

CRediT authorship contribution statement

Zhenchen Zhu: Writing – original draft, Methodology, Formal analysis, Conceptualization. **Ge Hu:** Writing – original draft, Visualization, Validation, Software, Data curation. **Zhoumeng Ying:** Writing – original draft, Visualization, Validation. **Jinhua Wang:** Writing – original draft, Methodology, Investigation. **Wei Han:** Writing – review & editing, Methodology, Investigation. **Zhengsong Pan:** Writing – review & editing, Software, Resources. **Xinlun Tian:** Writing – review & editing, Investigation, Funding acquisition, Data curation. **Wei Song:** Writing – review & editing, Visualization, Data curation. **Xin Sui:** Writing – review & editing, Visualization, Resources, Project administration. **Lan Song:** Writing – review & editing, Visualization, Validation, Supervision, Data curation, Conceptualization. **Zhengyu Jin:** Resources, Project administration, Investigation, Funding acquisition.

Declaration of competing interest

The authors declare that they have no known competing financial interests or personal relationships that could have appeared to influence the work reported in this paper.

Acknowledgments

We thank LetPub (www.letpub.com) for its linguistic assistance during the preparation of this manuscript.

Appendix A. Supplementary data

Supplementary data to this article can be found online at https://doi.org/10.1016/j.heliyon.2024.e27963.

References

[1] T. Burki, WHO ends the COVID-19 public health emergency, Lancet Respir. Med. 11 (7) (July 2023) 588, https://doi.org/10.1016/S2213-2600(23)00217-5.
[2] G. Herpe, et al., Efficacy of chest CT for COVID-19 pneumonia diagnosis in France, Radiology 298 (2) (2021) E81–E87, https://doi.org/10.1148/radiol.2020202568.
[3] K. Li, et al., The clinical and chest CT features associated with severe and critical COVID-19 pneumonia, Invest. Radiol. 55 (6) (2020) 327–331, https://doi.org/10.1097/RLI.0000000000000672.
[4] P. Lyu, et al., The performance of chest CT in evaluating the clinical severity of COVID-19 pneumonia: identifying critical cases based on CT characteristics, Invest. Radiol. 55 (7) (2020) 412–421, https://doi.org/10.1097/RLI.0000000000000689.
[5] D.E. Tekcan Sanli, et al., Predictive value of CT imaging findings in COVID-19 pneumonia at the time of first-screen regarding the need for hospitalization or intensive care unit, Diagn. Interv. Radiol. 27 (5) (2021) 599–606, https://doi.org/10.5152/dir.2020.20421.
[6] R. Yang, et al., Chest CT severity score: an imaging tool for assessing severe COVID-19, Radiol. Cardiothorac. Imaging 2 (2) (2020) e200047, https://doi.org/10.1148/ryct.2020200047.
[7] M.E. Laino, et al., Prognostic findings for ICU admission in patients with COVID-19 pneumonia: baseline and follow-up chest CT and the added value of artificial intelligence, Emerg. Radiol. 29 (2) (2022) 243–262, https://doi.org/10.1007/s10140-021-02008-y.
[8] M. Francone, et al., Chest CT score in COVID-19 patients: correlation with disease severity and short-term prognosis, Eur. Radiol. 30 (12) (2020) 6808–6817, https://doi.org/10.1007/s00330-020-07033-y.
[9] N.J. Polyakov, et al., Rate of true-positive findings of COVID-19 typical appearance at chest CT per RSNA Consensus guidelines in an increasingly vaccinated population, Radiology 306 (3) (2023) e220680, https://doi.org/10.1148/radiol.220680.
[10] M.T. Tsakok, et al., Reduction in chest CT severity and improved hospital outcomes in SARS-CoV-2 Omicron compared with Delta variant infection, Radiology 306 (1) (2023) 261–269, https://doi.org/10.1148/radiol.220533.
[11] A. Crombe, et al., Impact of vaccination and the Omicron variant on COVID-19-related chest CT findings: a multicenter study, Radiology 307 (3) (2023) e222730, https://doi.org/10.1148/radiol.222730.
[12] E. Charpentier, et al., Visual lung damage CT score at hospital admission of COVID-19 patients and 30-day mortality, Eur. Radiol. 31 (11) (2021) 8354–8363, https://doi.org/10.1007/s00330-021-07938-2.
[13] A.H. Elmokadem, et al., Comparison of chest CT severity scoring systems for COVID-19, Eur. Radiol. 32 (5) (2022) 3501–3512, https://doi.org/10.1007/s00330-021-08432-5.
[14] A. Bernheim, et al., Chest CT findings in coronavirus disease-19 (COVID-19): relationship to duration of infection, Radiology 295 (3) (2020) 200463, https://doi.org/10.1148/radiol.2020200463.
[15] S.M. Erturk, et al., Covid-19: correlation of early chest computed tomography findings with the course of disease, J. Comput. Assist. Tomogr. 44 (5) (2020) 633–639, https://doi.org/10.1097/RCT.0000000000001073.
[16] Z. Luo, et al., Association between chest CT features and clinical course of Coronavirus Disease 2019, Respir. Med. 168 (2020) 105989, https://doi.org/10.1016/j.rmed.2020.105989.

[17] J.J. Zhang, et al., Risk and protective factors for COVID-19 morbidity, severity, and mortality, Clin. Rev. Allergy Immunol. 64 (1) (2023) 90–107, https://doi.org/10.1007/s12016-022-08921-5.
[18] Y. Chen, et al., Aging in COVID-19: vulnerability, immunity and intervention, Ageing Res. Rev. 65 (2021) 101205, https://doi.org/10.1016/j.arr.2020.101205.
[19] Xinhua, COVID-19 Response Further Optimized with 10 New Measures, 2022 [cited 2023 March 13]; Available from: https://english.www.gov.cn/statecouncil/ministries/202212/08/content_WS63913c92c6d0a757729e4135.html.
[20] K. Leung, et al., Estimating the transmission dynamics of SARS-CoV-2 Omicron BF.7 in Beijing after adjustment of the zero-COVID policy in November-December 2022, Nat. Med. (2023), https://doi.org/10.1038/s41591-023-02212-y.
[21] Y. Pan, et al., Characterisation of SARS-CoV-2 variants in Beijing during 2022: an epidemiological and phylogenetic analysis, Lancet 401 (10377) (2023) 664–672, https://doi.org/10.1016/S0140-6736(23)00129-0.
[22] National Health Commission of the People's Republic of China, Guidelines for the Diagnosis and Treatment of COVID-19 *(10th Trial Version)*, 2023 [cited 2023 March 13], http://www.gov.cn/zhengce/zhengceku/2023-01/06/5735343/files/5844ce04246b431dbd322d8ba10afb48.pdf (in Chinese).
[23] S. Simpson, et al., Radiological society of North America Expert Consensus statement on reporting chest CT findings related to COVID-19. Endorsed by the Society of Thoracic Radiology, the American College of Radiology, and RSNA - secondary publication, J. Thorac. Imag. 35 (4) (2020) 219–227, https://doi.org/10.1097/RTI.0000000000000524.
[24] D.M. Hansell, et al., Fleischner Society: glossary of terms for thoracic imaging, Radiology 246 (3) (2008) 697–722, https://doi.org/10.1148/radiol.2462070712.
[25] Q.Q. Zhu, et al., Pulmonary artery trunk enlargement on admission as a predictor of mortality in in-hospital patients with COVID-19, Jpn. J. Radiol. 39 (6) (2021) 589–597, https://doi.org/10.1007/s11604-021-01094-9.
[26] M. Erdogan, et al., Prognostic utility of pulmonary artery and ascending aorta diameters derived from computed tomography in COVID-19 patients, Echocardiography 38 (9) (2021) 1543–1551, https://doi.org/10.1111/echo.15170.
[27] R.D. Riley, et al., Calculating the sample size required for developing a clinical prediction model, BMJ 368 (2020) m441, https://doi.org/10.1136/bmj.m441.
[28] J.E. Lee, et al., Imaging and clinical features of COVID-19 breakthrough infections: a multicenter study, Radiology 303 (3) (2022) 682–692, https://doi.org/10.1148/radiol.213072.
[29] E. Askani, et al., Computed tomographic imaging features of COVID-19 pneumonia caused by the Delta (B.1.617.2) and Omicron (B.1.1.529) variant in a German Nested Cohort Pilot Study Group, Tomography 8 (5) (2022) 2435–2449, https://doi.org/10.3390/tomography8050202.
[30] G. Lu, et al., Geriatric risk and protective factors for serious COVID-19 outcomes among older adults in Shanghai Omicron wave, Emerg. Microb. Infect. 11 (1) (2022) 2045–2054, https://doi.org/10.1080/22221751.2022.2109517.
[31] C.P. Ong, et al., Comparative analysis of SARS-CoV-2 Omicron BA.2.12.1 and BA.5.2 variants, J. Med. Virol. 95 (1) (2023) e28326, https://doi.org/10.1002/jmv.28326.
[32] P. Qu, et al., Enhanced neutralization resistance of SARS-CoV-2 Omicron subvariants BQ.1, BQ.1.1, BA.4.6, BF.7, and BA.2.75.2, Cell Host Microbe 31 (1) (2023) 9–17. e3, https://doi.org/10.1016/j.chom.2022.11.012.
[33] A. Tuekprakhon, et al., Antibody escape of SARS-CoV-2 Omicron BA.4 and BA.5 from vaccine and BA.1 serum, Cell 185 (14) (2022) 2422–2433. e13, https://doi.org/10.1016/j.cell.2022.06.005.
[34] W.H. Chong, et al., The incidence of pleural effusion in COVID-19 pneumonia: state-of-the-art review, Heart Lung 50 (4) (2021) 481–490, https://doi.org/10.1016/j.hrtlng.2021.02.015.
[35] A.H. Al-Tarbsheh, et al., Pericardial effusion in COVID-19 patients, Am. J. Med. Sci. 364 (1) (2022) 129–130, https://doi.org/10.1016/j.amjms.2022.01.024.
[36] L. Zhang, et al., CT imaging features of 34 patients infected with COVID-19, Clin. Imag. 68 (2020) 226–231, https://doi.org/10.1016/j.clinimag.2020.05.016.
[37] T.C. Kwee, R.M. Kwee, Chest CT in COVID-19: what the radiologist needs to know, Radiographics 40 (7) (2020) 1848–1865, https://doi.org/10.1148/rg.2020200159.
[38] A. Poerio, et al., Halo, reversed halo, or both? Atypical computed tomography manifestations of coronavirus disease (COVID-19) pneumonia: the "double halo sign", Korean J. Radiol. 21 (10) (2020) 1161–1164, https://doi.org/10.3348/kjr.2020.0687.
[39] A. Devie, et al., COVID-19: a qualitative chest CT model to identify severe form of the disease, Diagn. Interv. Imaging 102 (2) (2021) 77–84, https://doi.org/10.1016/j.diii.2020.12.002.
[40] J.C. Hogg, Role of latent viral infections in chronic obstructive pulmonary disease and asthma, Am. J. Respir. Crit. Care Med. 164 (10 Pt 2) (2001) S71–S75, https://doi.org/10.1164/ajrccm.164.supplement_2.2106063.
[41] H.C. Chuang, et al., Alteration in angiotensin-converting enzyme 2 by PM(1) during the development of emphysema in rats, ERJ Open Res. 6 (4) (2020), https://doi.org/10.1183/23120541.00174-2020.
[42] J.P. Kanne, et al., Long-term lung abnormalities associated with COVID-19 pneumonia, Radiology 306 (2) (2023) e221806, https://doi.org/10.1148/radiol.221806.